Spatial and Temporal Patterns of Chlorophyll Concentration in the Southern California Bight

SCCWRP #0998

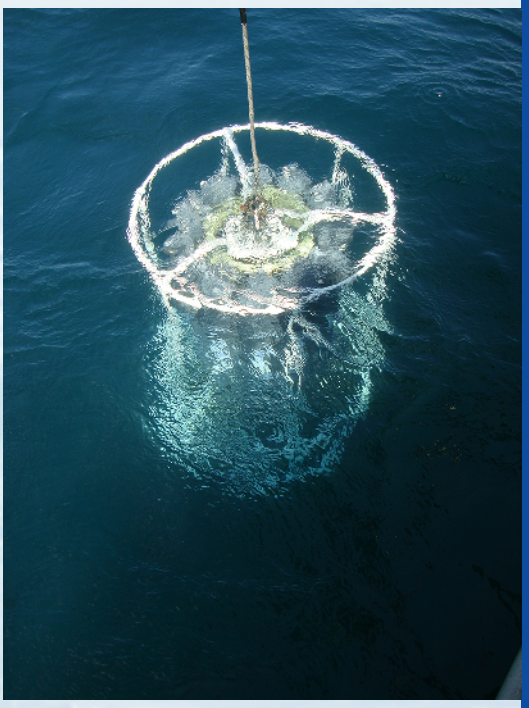

Nikolay P. Nezlin
Karen McLaughlin
J. Ashley T. Booth
Curtis L. Cash
Dario W. Diehl
Kristen Davis
Adriano Feit
Ralf Goericke
Joseph R. Gully
Meredith D.A. Howard
Scott Johnson
Ami Latker
Michael J. Mengel
George L. Robertson
Alex Steele
Laura Terriquez
Libe Washburn
Stephen B. Weisberg

Southern California Coastal Water Research Project

Technical Report 998

Spatial and Temporal Patterns of Chlorophyll Concentration in the Southern California Bight

Nikolay P. Nezlin[1], Karen McLaughlin[1], J. Ashley T. Booth[2], Curtis L. Cash[2], Dario W. Diehl[1], Kristen Davis[3], Adriano Feit[4], Ralf Goericke[5], Joseph R. Gully[6], Meredith D.A. Howard[1], Scott Johnson[7], Ami Latker[4], Michael J. Mengel[8], George L. Robertson[8], Alex Steele[6], Laura Terriquez[8], Libe Washburn[9], Stephen B. Weisberg[1]

[1]Southern California Coastal Water Research Project
[2]City of Los Angles Sanitation
[3]University of California, Irvine
[4]Public Utilities Department, City of San Diego
[5]Scripps Institution of Oceanography
[6] Sanitation Districts of Los Angeles County
[7]Aquatic Bioassay Consulting Laboratories
[8]Orange County Sanitation District
[9]University of California, Santa Barbara

August 2017
Technical Report 998

EXECUTIVE SUMMARY

Distinguishing between local, anthropogenic nutrient inputs and large-scale climatic forcing as drivers of coastal phytoplankton biomass is critical to developing effective nutrient management strategies. Here we assess the relative importance of these two drivers by comparing trends in chlorophyll-*a* in coastal (0.1–16.5 km) to offshore (17–700 km) areas, hypothesizing that coastal regions influenced by anthropogenic nutrient inputs would have different spatial and temporal patterns in chlorophyll-*a* concentration from offshore regions where coastal inputs are less influential. Quarterly CTD fluorescence measurements collected from three southern California continental shelf regions since 1998 were compared to chlorophyll-*a* data from the more offshore California Cooperative Fisheries Investigations (CalCOFI) program during the same period. We found the trends in the coastal zone were comparable to those offshore, with a gradual increase in total chlorophyll-*a* and a shallowing of the subsurface chlorophyll-*a* maximum depth since the beginning of observations, followed by chlorophyll-*a* declining and deepening from 2010 to present. An exception was the northern coastal part of SCB, where chlorophyll-*a* continued increasing after 2010. The observed trends appear to be strongly associated with ocean physical environment. The long-term increase in chlorophyll-*a* prior to 2010 was correlated with increased nitrate concentrations in deep waters, while the recent decline was associated with deepening of the upper mixed layer. The observed trends in chlorophyll-*a* appear to be linked to the low-frequency climatic cycles of the Pacific Decadal Oscillation and North Pacific Gyre Oscillation. These large-scale factors affecting the physical structure of the water column may also influence the biological response to terrestrially derived nutrient sources, making it difficult to distinguish the effects of anthropogenic inputs on chlorophyll along the coast.

TABLE OF CONTENTS

TABLE OF FIGURES

INTRODUCTION

Remotely-sensed ocean color data suggest that phytoplankton biomass has been increasing along the southern California coast over the last several decades [*Kahru et al.*, 2012; *Nezlin et al.*, 2012]. Such increases can result from local nutrient inputs [*Howard et al.*, 2014], but can also result from large-scale climate forcing [*Cloern*, 2001]. For instance, natural processes like strengthening of wind-generated coastal upwelling [*Bakun*, 1990; *Bakun et al.*, 2010; *Di Lorenzo*, 2015] and increased nutrient concentrations in deep source waters [*Rykaczewski and Dunne*, 2010; *Bograd et al.*, 2015] can affect frequency and magnitude of algal blooms nearshore. Large-scale climatic drivers affecting phytoplankton biomass in the northeastern Pacific, including enhanced stratification due to global warming and decreasing productivity [*Behrenfeld et al.*, 2006; *Polovina et al.*, 2008], are linked to low-frequency events like the El-Niño Southern Oscillation (ENSO) [*Philander*, 1990; *Trenberth*, 1997] and regime shifts thereof [*Hayward et al.*, 1999; *Miller and Schneider*, 2000; *Peterson and Schwing*, 2003; *Kim and Miller*, 2007], and climatic cycles like the Pacific Decadal Oscillation (PDO) [*Mantua et al.*, 1997; *Newman et al.*, 2016] and the North Pacific Gyre Oscillation (NPGO) [*Di Lorenzo et al.*, 2008].

Ocean physical environment has a strong control over primary producer response. Phytoplankton growth is regulated by the availability of light and nutrients, with most of nutrient supply to well-illuminated surface ocean coming from the mixing and upwelling of cold, nutrient-rich water from below [*Longhurst*, 1995; *Longhurst*, 1998]. Enhanced stratification can suppress nutrient exchange through vertical mixing, while surface cooling favors elevated vertical exchange which may result in greater primary productivity.

Differentiating between the effects of local eutrophication from coastal anthropogenic nutrient inputs and climate forcing is important for successful coastal resource management. Here, we assess the relative importance of these two drivers by comparing trends in chlorophyll in three coastal regions of the Southern California Bight (SCB) subject to nutrient pollution, with trends farther offshore, where anthropogenic nutrients are not expected to play a significant role. Specifically, we examine interannual trends in chlorophyll vertical structure and physical environment in the nearshore zone (0.1–16.5 km offshore) with the offshore region (17–700 km) utilizing decades-long records of *in situ* observations of chlorophyll to better understand the relative role of global versus local controls on the long-term trends in phytoplankton biomass in the SCB.

METHODS

Data collection

Nearshore SCB chlorophyll fluorescence profiles were measured quarterly at 258 stations along *49* cross-shelf transects from summer 1998–fall 2015 in the northern and central SCB and from fall 2003–fall 2015 in the southern SCB (Figure 1). CTDs were deployed to 100 m depth, or to 2 m above the bottom at stations with less than 100 m depth, measuring a suite of ocean properties including pressure, temperature, salinity, colored dissolved organic matter, dissolved oxygen, and chlorophyll fluorescence. The resulting 8 Hz or 24 Hz profiles were averaged to 1 m bins.

Sampling was conducted by five Publicly Owned Treatment Works (POTW) agencies, each using their own instruments and vessels: Aquatic Bioassay and Consulting Laboratories, Inc., representing the City of Oxnard (Oxnard), City of Los Angeles (CLA), Los Angeles County Sanitation Districts (LACSD), Orange County Sanitation District (OCSD), and City of San Diego (CSD). For analysis, we grouped data regionally, Oxnard and CLA as the northern region, LACSD and OCSD as the central region, and CSD as the southern coastal region (Figure 1).

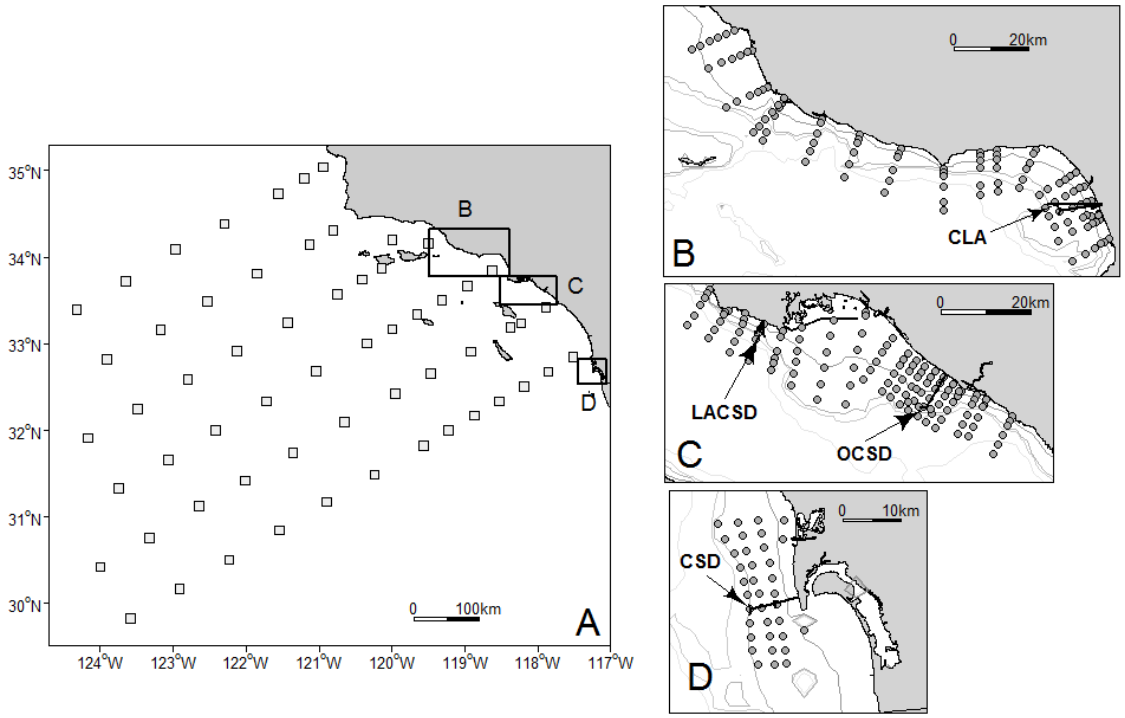

Figure 1. (A) CalCOFI stations and the (B) northern; (C) central; (D) southern coastal SCB regions where CTD profiles were collected during POTW WQ monitoring. Arrows point at the four major wastewater outfalls in SCB: City of Los Angeles (CLA), Los Angeles County Sanitation District (LACSD), Orange County Sanitation District (OCSD) and City of San Diego (CSD).

Chlorophyll florescence measurements were made with WetStar WS3S fluorometers, which were calibrated annually by the manufacturer. Conversion of chlorophyll fluorescence to chlorophyll-*a* concentration (CHL) was based on 357 discrete CHL samples collected from the surface and the maximum CHL fluorescence layer in parallel to CTD profiles in winter 2009 (70 samples), winter 2010 (24 samples), spring 2010 (211 samples) and spring 2013 (52 samples). Calibration samples were collected in the morning to minimize the effect of diurnal variations of CHL fluorescence yield. CHL was extracted in 90% acetone and measured with a Turner 10-AU fluorometer using the acidification method [*Parsons et al.*, 1984]. A power relationship between discrete CHL concentration (mg m^{-3}) and fluorescence (volts) was developed from these data:

$$[CHL = 5.8423 \cdot V^{1.0649}], \qquad \text{(Eq. 1)}$$

and applied to all data since 2009. A power relationship was preferred over linear because statistical distribution of CHL in the ocean is typically close to lognormal [*Banse and English*, 1994; *Campbell*, 1995]. The relationship demonstrated high correlation ($R^2 = 0.677$) and was equally applicable to all southern California regions and observation periods (no significant differences were detected by ANOVA).

Prior to 2009, historical POTW CTD datasets did not include a voltage for CHL fluorescence and consequently the above relationship could not be applied. For these data CHL concentrations (mg m^{-3}) were calculated from fluorescence using standard linear coefficients provided by the manufacturer. Factory calibration ensures the scaling factor correctly responds to internal standards and reference lab culture of *Thalassiosira weissflogii* phytoplankton used by the manufacturer, in addition to setting the clean water offset. However, comparison of the CHL concentration reported using the manufacturer calibration and discrete bottle samples collected as calibration for this study showed that the manufacturer calibration significantly overestimated chlorophyll concentrations in the SCB. Consequently, a correction factor of 0.4 was calculated as the averaged difference between all CHL bottle samples and corresponding factory-calibrated CTD CHL measurements and applied to the historical dataset. This difference in methodology converting fluorescence to chlorophyll concentration may influence the results. However, for the northern and central regions, the pre-2009 and post-2009 appear to align well, suggesting that difference in methodology did not significantly affect the data. However, the data for the southern region appears to have an abrupt change, which may be due to the change in methodology rather than chlorophyll biomass. In general, pre-2009 data should be interpreted with caution.

Oceanographic observations offshore of southern California have been carried out for almost 70 years by the CalCOFI program (www.calcofi.org). It includes regular collection of discrete samples of inorganic nutrients and CHL detected by chemical methods resulting in measurements more accurate than nearshore data of POTW monitoring. Since 1984, concentrations of inorganic nutrients and CHL, as well as basic hydrographic variables, have been measured on a quarterly basis at 59 stations off Southern California (Figure 1A) in an area extending almost 700 km offshore (referred below as CalCOFI region). Data at each station included *in situ* water samples collected by 10-L plastic Niskin bottles typically at 20 depths, generally chosen to provide high resolution (~10 m) around the subsurface CHL maximum and the shallow salinity minimum of the upper thermocline. Temperature, salinity, and inorganic nutrients (including nitrate) were measured for all depths sampled. CHL samples were taken within the upper 200 m or within lesser depths at shallower stations and CHL was determined from the fluorescence of acetone extracts [*Parsons et al.*, 1984]. Further details of the sampling and analytical procedures can be found at www.calcofi.org.

Analytical metrics

Two metrics were used to assess spatial and temporal trends in magnitude and vertical structure of phytoplankton biomass at each station. To ascertain changes in the magnitude of biomass, we calculated vertically-integrated CHL concentration of the water column CHL_{tot} (mg CHL m^{-2})

$$CHL_{tot} = \int CHL(z) \cdot dZ \qquad \text{(Eq.2)}$$

where CHL(z) is CHL concentration (mg CHL m^{-3}) at depth Z.

To evaluate changes in vertical structure we calculated the depth of the CHL profiles' center of mass, D_{chl} (m):

$$D_{chl}\ (\text{m}) = \frac{1}{CHL_{tot}} \cdot \int Z \cdot dCHL(z) \qquad \text{(Eq. 3)}$$

Center of mass was preferred over the more traditional chlorophyll maximum depth [cf. *Cullen*, 2015] because many nearshore profiles had two (or more) subsurface peaks in chlorophyll fluorescence or broad maximum peaks, making classification of a single "maximum" depth layer difficult.

We investigated three metrics to characterize the relationship between the ocean physical environment and CHL_{tot} and D_{chl} in the SCB: (1) water column stratification regulating nutrient flux into the euphotic zone, (2) nutrient concentration in deeper waters, (3) horizontal advection of waters with different nutrient content associated with large-scale ocean circulation patterns ("nutrient-rich" waters transported from the north vs. "nutrient-poor" waters from the south). To assess covariance of deep-water nutrients with CHL, the nitracline depth (D_{nc}) was calculated as the depth where nitrate concentrations started increasing with depth from near-zero (<0.1 µM L^{-1}) values (calculated for CalCOFI data only). The depth of the potential density anomaly (σ_θ) 25.0 kg m^{-3} isopycnal ($D_{\sigma 25}$) was used as a proxy for water column stratification. Isopycnal surface 25.0 kg m^{-3} was selected because this density was measured in most profiles of both CALCOFI and POTW datasets, and could thus be used as a characteristic of water column density profiles. $D_{\sigma 25}$ was preferred to other measures of water column stratification (buoyancy frequency and the pycnocline depth calculated using different methods [*Papadakis*, 1981; *Freeland et al.*, 1997; *Thomson and Fine*, 2003]), which demonstrated poor relationship with CHL_{tot} and D_{chl}. Spiciness π (a state variable uncorrelated with density [*Flament*, 2002]), is often used as a tracer of basin-scale water mass movements. We analyzed spiciness at the $D_{\sigma 25}$ depth ($\pi_{\sigma 25}$). All oceanographic parameters were calculated using the R package "oce" (http://dankelley.github.io/oce/documentation.html).

Statistical analysis

Temporal trends, and regions where these trends occurred, were assessed using Empirical Orthogonal Functions (EOFs) [*Preisendorfer*, 1988; *Emery and Thomson*, 2014]. EOFs decompose time series of spatial maps (here time series of CHL_{tot}, D_{chl}, etc. over the sampling patterns from the three POTW and one CALCOFI regions) into a set of orthogonal functions, or modes. These modes consist of two parts: (1) maps of spatial distributions of a variable for each mode; and (2) a time series that quantifies how each map changes in time. In the procedure, each parameter $\psi_m(t)$ (e.g. CHL_{tot}) at each station m time t was normalized as

$$\psi_m'(t) = [\ \psi_m(t) - \bar{\psi}_m\ ] / \sigma_m \qquad \text{(Eq. 4)}$$

where $\bar{\psi}_m$ and σ_m are the mean and standard deviation over all observations at station m. Variations of each parameter were separated into modes as,

$$\psi_m'(t) = \sum_i^M a_i'(t) \cdot \varphi_{im} \qquad \text{(Eq. 5)}$$

where $a_i'(t)$ is the amplitude function of mode i for observation t; φ_{im} is spatial mode i at station m; summation is over all M modes. Spatial modes φ_{ij} are orthogonal and amplitude functions

$a_i'(t)$ are uncorrelated. The modes are ranked according to the fraction of variance accounted for each mode in the original data. Often a few modes explain much of the variance for a given parameter. Missing data were reconstructed using the Data Interpolating Empirical Orthogonal Functions (DINEOF) approach [*Beckers and Rixen*, 2003] implemented in the R package "spacetime" [*Pebesma*, 2012]. Normalized amplitude functions $a_i'(t)$ obtained using Eq. 5 were transformed to dimensional amplitude functions $a_i(t)$ by regressing them against the original data set.

EOF analysis was applied independently to the three coastal SCB regions and the offshore CalCOFI region. For all parameters, only the first EOF mode (m = 1) was analyzed because it captured the fundamental variability of the system (27%–94%). Other EOF modes were not analyzed because they explained less variance and did not exhibit clear spatial patterns through time.

The periods when trends were statistically significant were detected using Generalized Additive Models (GAM), a method based on optimal smoothing of the time series. GAM is a non-parametric generalization of the linear regression model [*Hastie and Tibshirani*, 1986], where the usual linear function of a covariate is replaced with a sum of unspecified smooth functions determined by the data through iterative smoothing operations. After the GAM model was fitted for each seasonally adjusted time series using R package "mgcv" [*Wood*, 2016], the derivatives (slopes) and their standard errors (confidence intervals) were computed for each predicted point using the method of finite differences. The periods when these derivatives were significantly different from zero at the selected confidence level were defined as statistically significant trends [*Simpson*, 2014]. The points between the increasing and decreasing periods were detected as the points where the slope is zero. A salient feature of most observed parameters was the change of the trend direction observed between 2006–2010. Significance of the trends before and after this change was estimated by detecting the time when the change occurred preceding the most recent period of significant change and estimating the significance of the linear trends before and after this time.

Influence of large-scale climatic forcing on local CHL expression

The effect of climate fluctuations on the CHL biomass and vertical structure was analyzed using the PDO and NPGO indices obtained from the websites http://research.jisao.washington.edu/pdo/PDO.latest and http://www.oces.us/npgo/npgo.php.

RESULTS

CHL biomass and vertical structure nearshore and offshore

Interannual variations of CHL_{tot} and D_{chl} nearshore and offshore generally demonstrated similar, but inverse, features. Offshore, in the CalCOFI region, CHL_{tot} increased and D_{chl} shoaled from the beginning of regular observations in 1984 to ~2006, followed by a decrease of CHL_{tot} starting in 2006 and a deepening of the D_{chl} starting in 2010 (Figure 2). On average, CHL_{tot} in the CalCOFI region increased from 34 mg m^{-2} in 1984 to 55 mg m^{-2} in 2006 and then decreased to 43 mg m^{-2} in 2015. The decrease since 2010 of CHL_{tot} was also observed in the central and

southern coastal SCB (Figure 3C–F), where CHL_{tot} decreased from 75–170 mg m^{-2} in 2010 to 45–59 mg m^{-2} in 2015, but not in the northern SCB where values continued to increase, from 32 mg m^{-2} in 1998 to 110 mg m^{-2} in 2015 (Figure 3B). No significant increase of CHL_{tot} before 2010 was observed in the central and southern regions (Figure 3C–F). Analyzing CHL_{tot} trends nearshore, we must consider the difference between the methods of CHL biomass assessment before and after 2009. The continuity in the time series of CHL_{tot} in the northern and central SCB suggests there may not be a bias from the methodological differences (Figure 3B, D). However, in the southern region, the lack of continuity between datasets suggests it could be the reason for the abrupt CHL_{tot} increase between 2008 and 2010 (Figure 3F).

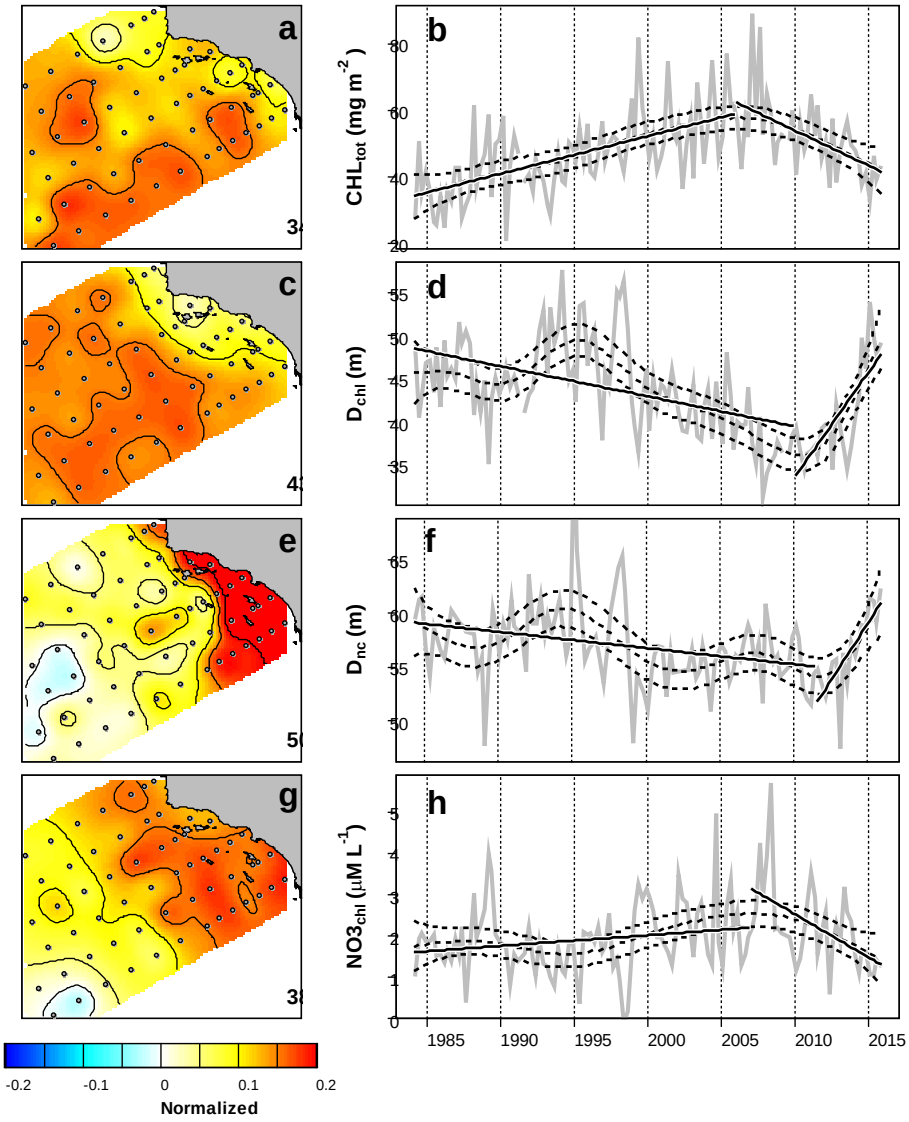

Figure 2. Spatial distributions (A, C, E, G) and temporal variations (B, D, F, H) of first EOF modes of integrated CHL (CHL_{tot}), CHL center of mass depth (D_{chl}), the depth of nitracline D_{nc} and nitrate concentration ($NO3_{chl}$) at the D_{chl} depth in CalCOFI region. The percent of variance explained by each mode is given at corner of the map. All time-series are smoothed using GAM-method (dashed lines show the mean and the 0.95 confidence interval). Black lines indicate the periods of significant ($p<0.05$) linear trends.

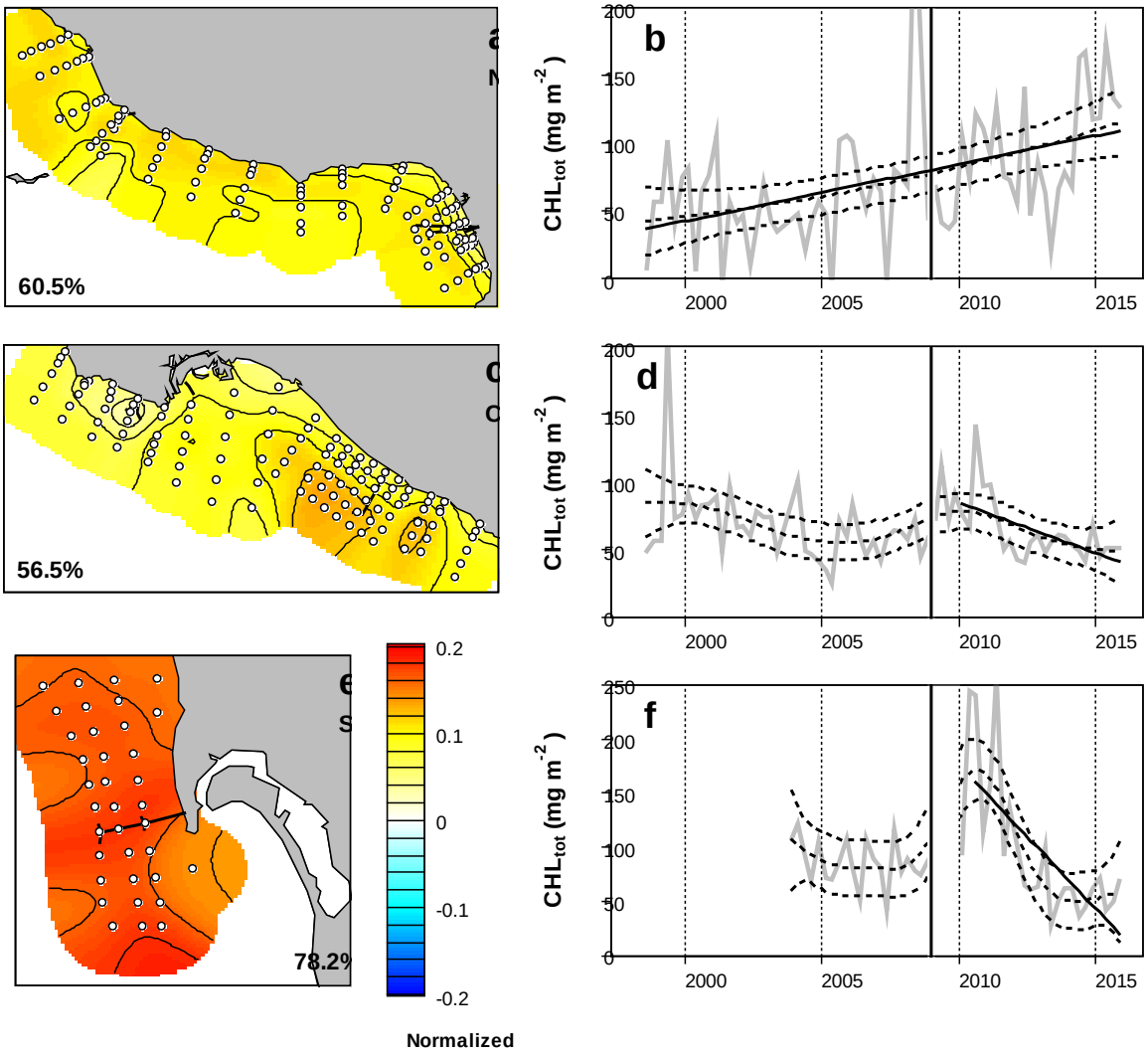

Figure 3. Spatial distributions (A, C, E) and temporal variations (B, D, F) of first EOF modes of the integrated CHL (CHL_{tot}) in northern (A, B), central (C, D), and southern (E, F) coastal regions (POTW dataset). The percent of variance explained by each mode is given at corner of the map. All time-series are smoothed using GAM-method (dashed lines show the mean and the 0.95 confidence interval). Black lines indicate the periods of significant ($p<0.05$) linear trend. Vertical lines indicate the time (2009) when the method of CHL calculation was changed.

The deepening of D_{chl} after 2006–2010 observed offshore (Figure 2D) was also observed in all three coastal regions (Figure 4). In the northern and central coastal regions, D_{chl} was 18–21 m in 2006–2011 and deepened to 22–25 m in 2015 (Figure 4B, D), whereas in the southern region D_{chl} deepened from 25 m in 2008–2011 to 36 m in 2015 (Figure 4F). In the CalCOFI region, D_{chl} deepened from 36 m in 2010 to 48–50 m in 2015 (Figure 2D). Before 2010, significant shallowing of the D_{chl} was observed offshore and in the central coastal SCB (Figure 2D, 4D). In the northern and southern SCB this trend was insignificant (Figure 4A, B, E, F), possibly due to short period of observations. Spatial distribution of the first EOF mode of D_{chl} in the CalCOFI region demonstrated higher variability offshore than nearshore (Figure 2C).

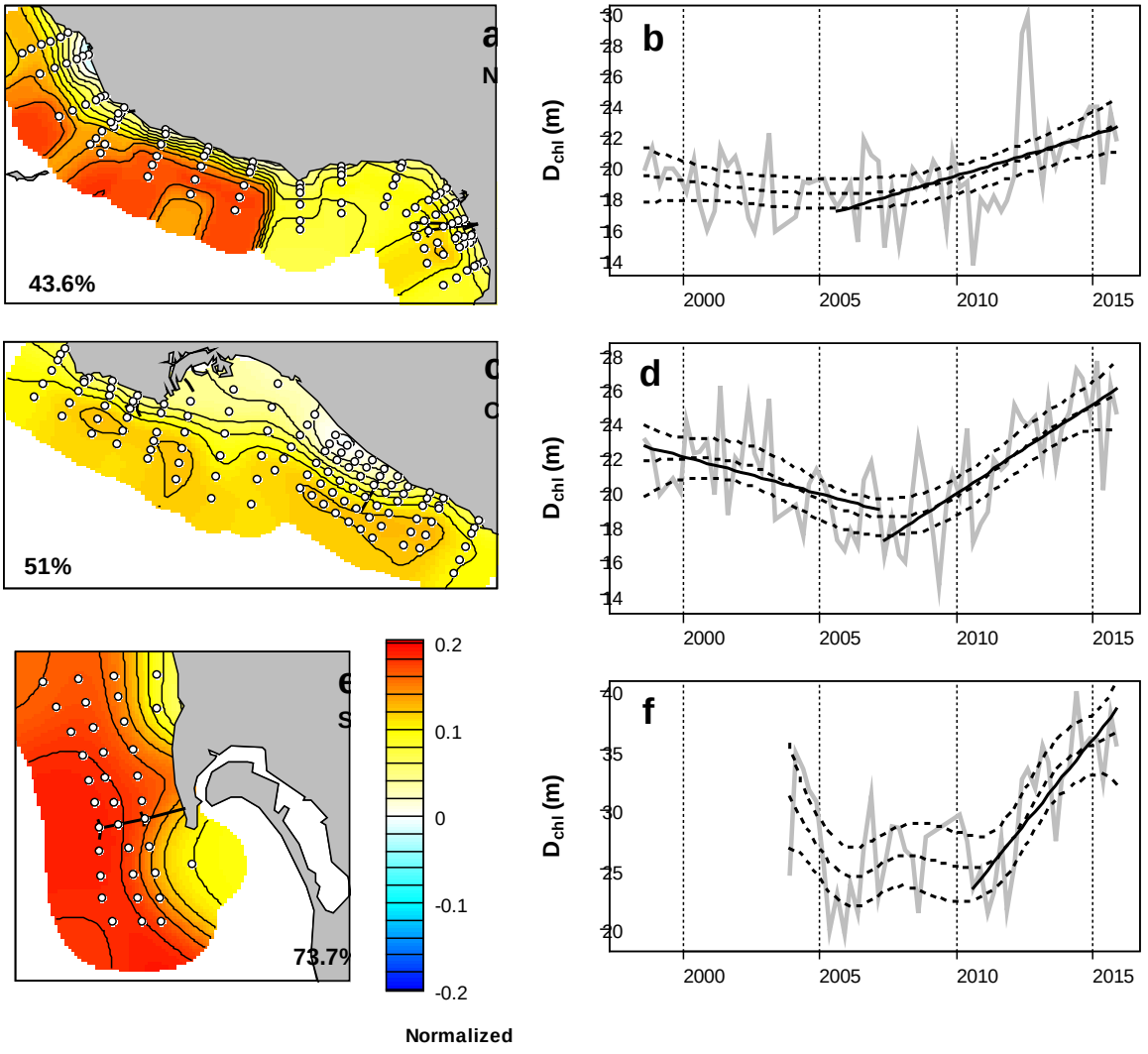

Figure 4. Spatial distributions (A, C, E) and temporal variations (B, D, F) of first EOF modes of the CHL center of mass depth (D_{chl}) in northern (A, B), central (C, D), and southern (E, F) coastal regions (POTW dataset). The percent of variance explained by each mode is given at corner of the map. All time-series are smoothed using GAM-method (dashed lines show the mean and the 0.95 confidence interval). Black lines indicate the periods of significant ($p<0.05$) linear trend.

Relationship with nutrients

Patterns in subsurface chlorophyll were highly correlated with nutrient availability in the offshore region (this could not be assessed from the nearshore POTW dataset). Changes in CHL_{tot} and D_{chl} during 1984–2010 covaried with the nitrate concentrations at the D_{chl} depth and the depth of the nitracline (Figure 2). In the CalCOFI area, the depths of D_{chl} and D_{nc} were significantly positively correlated ($R^2 = 0.70$; d.f. = 5500; correlation based on all profiles where D_{chl} and D_{nc} were detected), both demonstrating shallowing during 1984–2010 and deepening around 1995 and after 2010. Furthermore, a gradual increase in nitrate concentration at the D_{chl} during 1984–2010 (Figure 2H) also coincided with increasing CHL_{tot}.

Relationship with the ocean physical environment

We investigated three metrics to characterize the relationship between the ocean physical environment and spatial and temporal patterns in CHL_{tot} and D_{chl} in the SCB: (1) water column stratification regulating nutrient flux into the euphotic zone, represented by the metric $D_{\sigma 25}$, (2) horizontal advection of waters with different spiciness and nutrient content associated with large-scale ocean circulation patterns (cold/fresh/"nutrient-rich" waters transported from the north vs. warm/salty/"nutrient-poor" waters from the south), represented by the metric $\pi_{\sigma 25}$, and (3) nutrient concentration in deeper waters, represented by the metric $NO3_{\sigma 25}$.

Water column stratification, as interpreted through the isopycnal surface 25.0 kg m^{-3}, $D_{\sigma 25}$ (Figure 5E–F, 6), covaried with observed patterns in CHL_{tot} and D_{chl} after 2010 but not before. $D_{\sigma 25}$ was comparatively stable with two periods of deepening: about 1995–2000 (offshore) and 2010–2015 (all four datasets); $D_{\sigma 25}$ variations in the CalCOFI region were more pronounced nearshore than offshore (Figure 5E). Both periods of deepening of the $D_{\sigma 25}$ coincided with deepening of the D_{chl} (Figure 2B, 4) and the nitracline (Figure 2F), although only the recent (2010–2015) deepening resulted in a decrease of CHL_{tot} (Figure 2B, 3D, F).

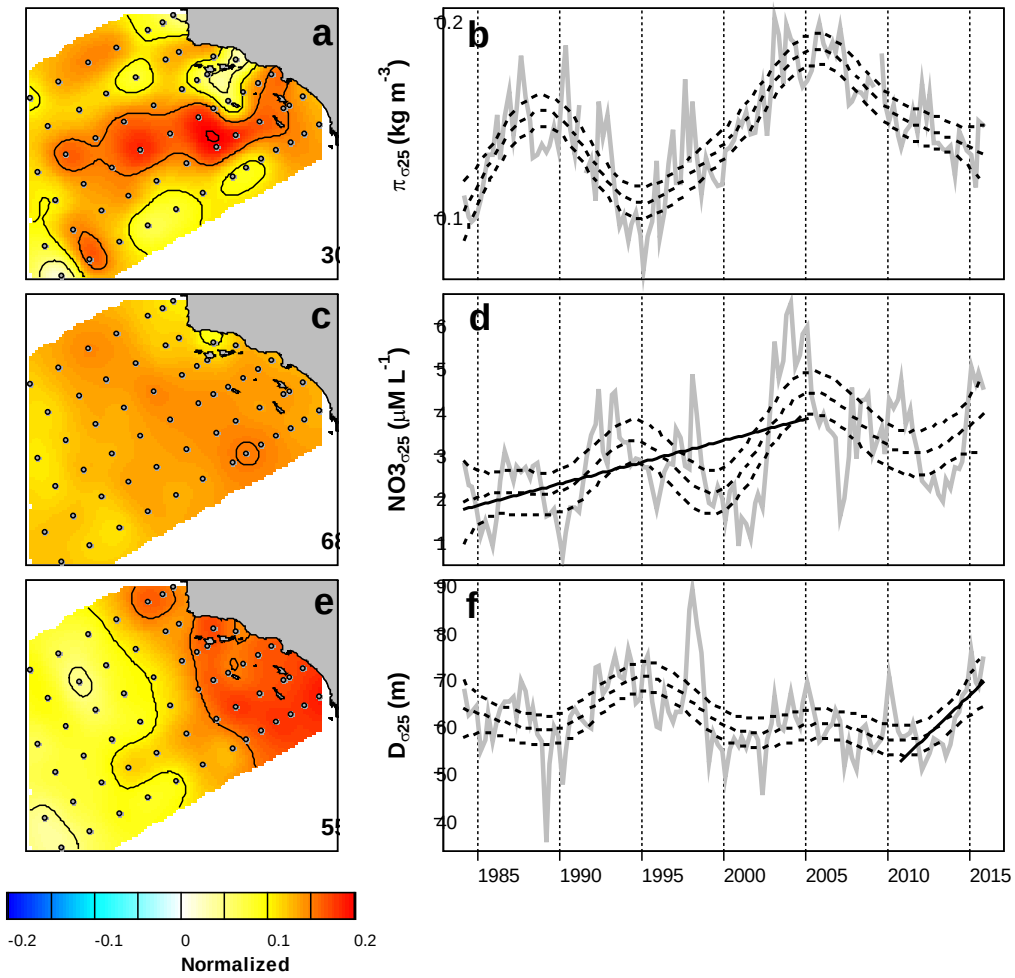

Figure 5. Spatial distributions (A, C, E, G) and temporal variations (B, D, F, H) of first EOF modes of spiciness $\pi_{\sigma 25}$ (A, B) and nitrate concentration $NO3_{\sigma 25}$ (C, D) at the depth of the 25.0 kg m^{-3} isopycnal and the depth $D_{\sigma 25}$ of this isopycnal (E, F) (CalCOFI dataset). The percent of variance explained by each mode is given at corner of the map. All time-series are smoothed using GAM-method (dashed lines show the mean and the 0.95 confidence interval). Black lines indicate the periods of significant ($p<0.05$) linear trend.

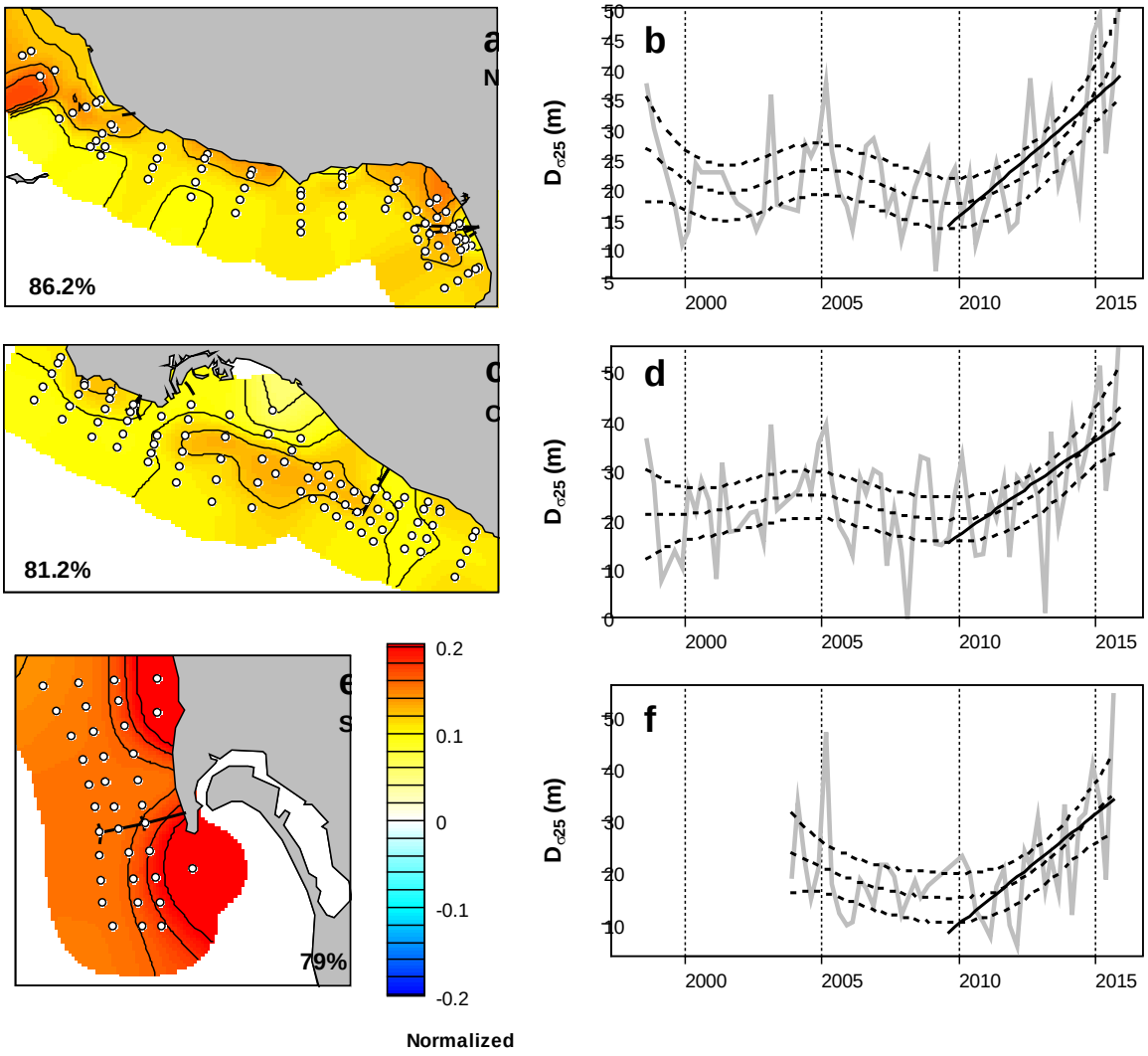

Figure 6. Spatial distributions (A, C, E) and temporal variations (B, D, F) of first EOF modes of the depth of the 25.0 kg m^{-3} isopycnal ($D_{\sigma 25}$) in the northern (A, B), central (C, D) and southern (E, F) coastal regions (POTW dataset). The percent of variance explained by each mode is given at corner of the map. All time-series are smoothed using GAM-method (dashed lines show the mean and the 0.95 confidence interval). Black lines indicate the periods of significant ($p<0.05$) linear trend.

Advection of waters of different origin, as interpreted through the metric spiciness, $\pi_{\sigma 25}$, did not seem to be associated with patterns in CHL_{tot} and D_{chl}. Temporal variations of $\pi_{\sigma 25}$ offshore and nearshore were similar (Figure 5A–B, 7), but there was no clear relationship between spiciness and CHL_{tot} and D_{chl} (cf. Figure 2B, D, 3, 4). In contrast to CHL_{tot} and D_{chl}, $\pi_{\sigma 25}$ demonstrated no significant linear trends during the observed period. Neither the spiciness maximum that occurred in 1997–1998 (associated with the strongest El Niño in the 20th century) nor the two spiciness minima in 1993 and 2004 were associated with maxima in either CHL_{tot} and D_{chl}.

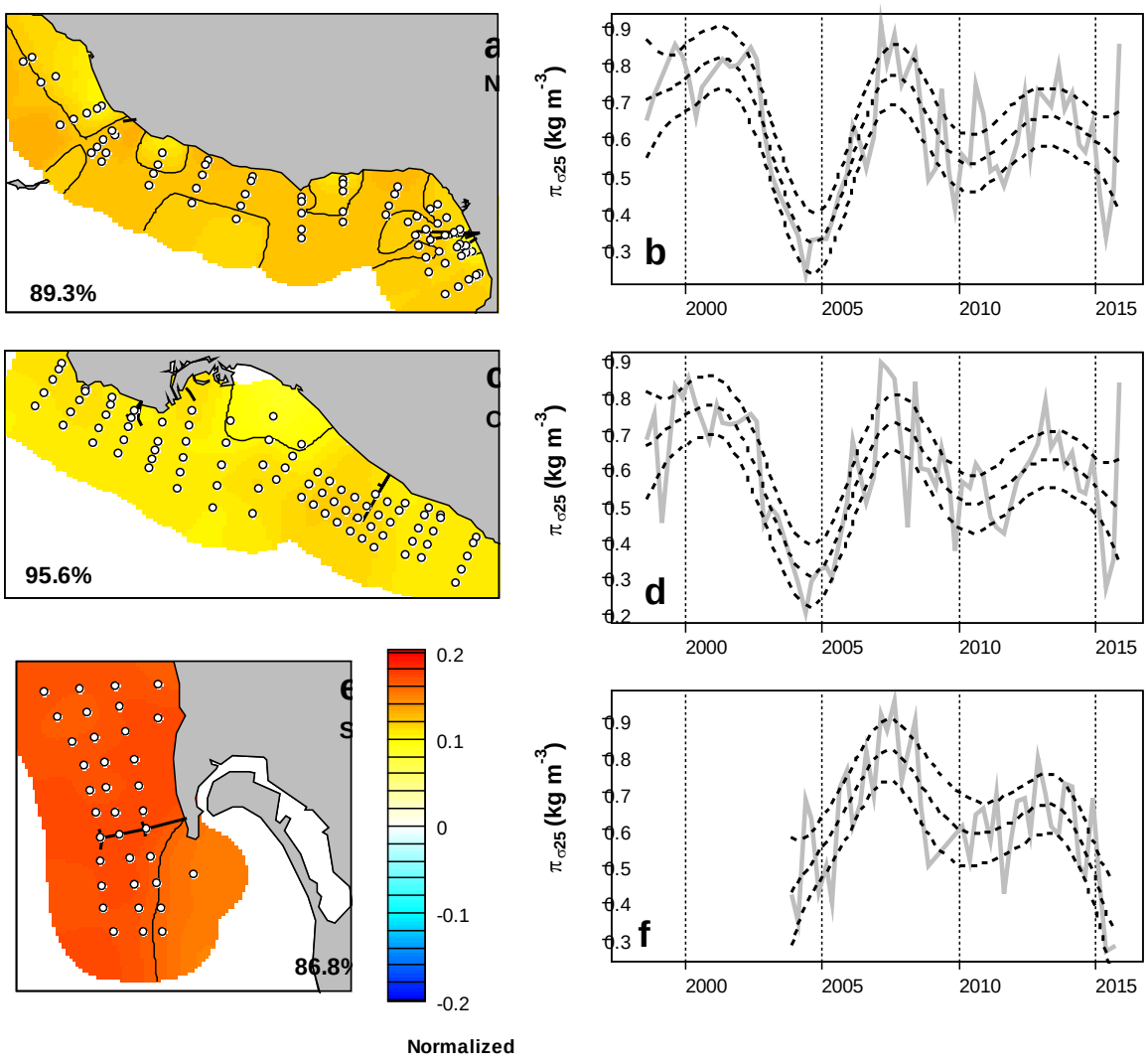

Figure 7. Spatial distributions (A, C, E) and temporal variations (B, D, F) of first EOF modes of spiciness at the depth of the 25.0 kg m^{-3} ($\pi_{\sigma 25}$) in the northern (A, B), central (C, D), and southern (E, F) coastal regions (POTW dataset). The percent of variance explained by each mode is given at corner of the map. All time-series are smoothed using GAM-method (dashed lines show the mean and the 0.95 confidence interval). Black lines indicate the periods of significant ($p<0.05$) linear trend.

Nitrate concentrations measured at the isopycnal surface 25.0 kg m^{-3}, $NO3_{\sigma 25}$, demonstrated two independent temporal patterns (Figure 5D). First, it was inversely correlated with spiciness, confirming the idea that cold/fresh waters advected from the north are rich in nutrients in contrast to warm/salty waters advected from the south. Similar temporal variations, however, are not seen in the CHL_{tot} and D_{chl}. Second, the nitrate concentrations at this depth (which was 10–30 m nearshore and 50–70 m offshore) significantly increased from 1984 to 2005 (Figure 5D), also observed as an increase in nitrate concentration at the depth of D_{chl} (Figure 2H).

DISCUSSION

The SCB, as a part of an eastern boundary current system, is strongly affected by seasonal coastal upwelling and the California Current transporting productive waters from the Subarctic Pacific [*Hickey*, 1979; *Lynn and Simpson*, 1987]. Others have noted that phytoplankton productivity in eastern boundary systems results from a combined effect of large-scale circulation and local factors [*Carr and Kearns*, 2003], and that multiple factors such as nutrient concentration, light availability, and water mass mixing can affect phytoplankton distribution [*Patti et al.*, 2008; *Messie and Chavez*, 2015]. The concurrence of nearshore and offshore trends in CHL biomass (CHL_{tot}) and vertical structure (D_{chl}) and their association with water column stratification ($D_{\sigma 25}$) and deep water nitrate concentrations suggest that nearshore subsurface CHL patterns are strongly influenced by Pacific Basin scale climate events.

Increasing CHL concentrations and shallowing of D_{chl} in the SCB during most of the observed period (1984–2010) appeared to be linked to a shallowing of the nitracline [*Aksnes and Ohman*, 2009; *Bjorkstedt et al.*, 2011; *McClatchie et al.*, 2016] and higher nitrate concentrations of deep waters that source upwelling [*Bjorkstedt et al.*, 2012; *Bograd et al.*, 2015]. Deep ocean nutrients are becoming enriched as a result of global changes related to ocean warming, including decreased ventilation of the North Pacific, more intensive remineralization at depth, and longer time for the water masses to accrue nitrate below the euphotic zone during their transits from the subarctic to the subtropics [*Rykaczewski and Dunne*, 2010]. In the SCB the effect of warming is different from the trends observed further offshore, where an increase in surface temperatures and stratification suppress nutrient supply to the euphotic zone making them less productive [*Roemmich and McGowan*, 1995; *Sarmiento et al.*, 2004; *Behrenfeld et al.*, 2006; *Steinacher et al.*, 2010; *Polovina et al.*, 2011].

The patterns in CHL_{tot} and D_{chl} and the associated physical factors appear to be linked to PDO and NPGO climatic cycles, which are forced responses of the ocean to atmospheric variability generated by the El Niño Southern Oscillation (ENSO) fluctuations in the Equatorial Pacific [*Di Lorenzo et al.*, 2013]. PDO and NPGO both drive upwelling, water transport, mixing, mesoscale structure, and ecosystem dynamics in the northeastern Pacific [*Mantua et al.*, 1997; *Di Lorenzo et al.*, 2009; *Di Lorenzo et al.*, 2013; *Kilduff et al.*, 2015]. The NPGO (defined as the second mode of sea surface height anomalies) is associated with the strength of the central and eastern parts of the North Pacific gyre, including the California Current [*Di Lorenzo et al.*, 2008], transporting productive ocean waters from the north. Previous studies demonstrated significant correlation between the NPGO index and surface chlorophyll-*a* [*Di Lorenzo et al.*, 2008] and

nitrate concentration in the upper mixed layer [*Di Lorenzo et al.*, 2009] averaged over the CalCOFI domain. The PDO (the leading mode of sea surface temperature variability in North Pacific) co-varies with different aspects of ocean ecosystems from Alaska to California, including salmon production regimes, continental surface air temperatures, major costal river flow, etc. [*Mantua et al.*, 1997]. In the northeastern Pacific Ocean, the periods of positive ("warm") PDO phases are associated with an El Niño-like increase of sea surface temperature, deepening of the pycnocline, and a decrease of primary production; while negative ("cold") PDO has an opposite effect [*Zhang et al.*, 1997; *Chao et al.*, 2000; *Wang et al.*, 2014]. The most pronounced effects on the ocean ecosystem (often called "physical-biological regime shifts") have occurred when the PDO and NPGO show strong, simultaneous, and opposite sign reversals [*Di Lorenzo et al.*, 2008].

During 1984–2010, both climatic indices (seasonally adjusted and smoothed by the GAM method) demonstrated small but significant trends (decreasing PDO and increasing NPGO) overlaid by quasi-periodic decadal oscillations (Figure 8). In the SCB, both these trends are associated with increased primary productivity. Starting in 2010, the PDO abruptly shifted from a cold to a warm phase, which in the northeastern Pacific resulted in enhanced stratification and a deepening of the upper mixed layer, thereby decreasing primary production, which we observed in our dataset.

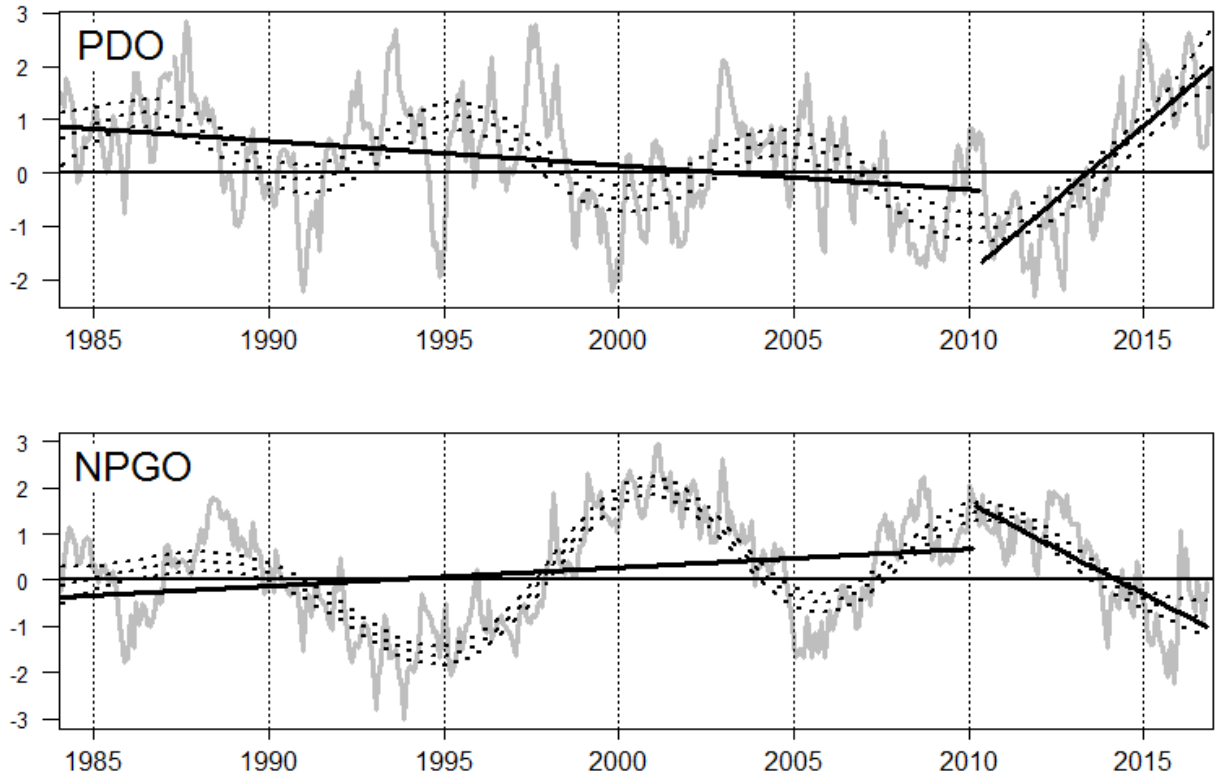

Figure 8. Pacific Decadal Oscillation (PDO) and North Pacific Gyre Oscillation (NPGO) smoothed by GAM-method (dashed lines show mean and 0.95 confidence interval). Black lines indicate the periods of significant (p<0.05) linear trend.

The effect of increasing PDO and decreasing NPGO on CHL in 2010–2015 was stronger than during a similar period around 1995, when the D_{chl} and nitracline deepened (cf. Figure 2D, F) but CHL_{tot} remained unchanged (Figure 2B). This may be linked to the increased range of PDO and NPGO fluctuations resulting from global warming [*Sydeman et al.*, 2013]. Other consequences of climate change in the study area may include the shoaling and strengthening of the California Undercurrent [*Meinvielle and Johnson*, 2013], a recent warm temperature anomaly in northeastern Pacific called "The Blob" [*Bond et al.*, 2015; *Di Lorenzo and Mantua*, 2016], and extremely dry weather in California starting 2011 with record drought in winter 2013/14.

The decrease of CHL_{tot} and deepening of D_{chl} during 2010-2015 was not observed in the northern coastal region of the SCB. Instead, CHL_{tot} in the northern region exhibited a weak, increasing trend over the entire time series between 1998–2005 (Fig. 3B). The most likely reason for this pattern is that this region, more than other parts of the SCB, is affected by advection of waters upwelled off Point Conception [*Hickey*, 1993; *Bray et al.*, 1999]. The trends of CHL_{tot} in the upwelling zone are expected to be different from the central and southern parts of the SCB, which look more similar to the open ocean because the SCB is sheltered from northerly upwelling-generating winds by a coastal mountain range [*Dorman and Winant*, 1995]. In contrast to the open ocean, the productivity of wind-generated coastal upwelling is expected to continue increasing [*Bakun*, 1990; *Bakun et al.*, 2010; *Di Lorenzo*, 2015].

This study demonstrated that climatic cycles in the North Pacific played a significant role in the dynamics of phytoplankton biomass in the southern California coastal zone, although this conclusion does not disregard local effect of anthropogenic nutrient inputs, which needs special analysis based on regular monitoring and numerical modeling.

REFERENCES

Aksnes, D.L., and M.D. Ohman (2009), Multi-decadal shoaling of the euphotic zone in the southern sector of the California Current System, *Limnology and Oceanography*, *54* (4), 1272-1281.

Bakun, A. (1990), Global climate change and intensification of coastal ocean upwelling, *Science*, *247*, 198-201.

Bakun, A., D.B. Field, A. Redondo-Rodriguez, and S.J. Weeks (2010), Greenhouse gas, upwelling-favorable winds, and the future of coastal ocean upwelling ecosystems, *Global Change Biology*, *16* (4), 1213-1228.

Banse, K., and D.C. English (1994), Seasonality of Coastal Zone Color Scanner phytoplankton pigment in the offshore oceans, *Journal of Geophysical Research-Oceans*, *99* (C4), 7323-7345.

Beckers, J.-M., and M. Rixen (2003), EOF calculations and data filling from incomplete oceanographic datasets, *Journal of Atmospheric and Oceanic Technology*, *20* (12), 1839-1856.

Behrenfeld, M.J., R.T. O'Malley, D.A. Siegel, C.R. McClain, J.L. Sarmiento, G.C. Feldman, A.J. Milligan, P.G. Falkowski, R.M. Letelier, and E.S. Boss (2006), Climate-driven trends in contemporary ocean productivity, *Nature*, *444* (7120), 752-755.

Bjorkstedt, E.P., R. Goericke, S. McClatchie, E. Weber, W. Watson, N. Lo, B. Peterson, B. Emmett, R. Brodeur, J. Peterson, M. Litz, J. Gomez-Valdez, G. Gaxiola-Castro, B. Lavaniegos, F. Chavez, C.A. Collins, J. Field, K. Sakuma, P. Warzybok, R. Bradley, J. Jahncke, S. Bograd, F. Schwing, G.S. Campbell, J. Hildebrand, W. Sydeman, S.A. Thompson, J.L. Largier, C. Halle, S.Y. Kim, and J. Abell (2011), State of the California Current 2010-2011: Regionally Variable Responses to a Strong (but Fleeting?) La Nina, *California Cooperative Oceanic Fisheries Investigations Reports*, *52*, 36-68.

Bjorkstedt, E.P., R. Goericke, S. McClatchie, E. Weber, W. Watson, N. Lo, W.T. Peterson, R.D. Brodeur, T. Auth, J. Fisher, C. Morgan, J. Peterson, J. Largier, S.J. Bograd, R. Durazo, G. Gaxiola-Castro, B. Lavaniegos, F.P. Chavez, C.A. Collins, B. Hannah, J. Field, K. Sakuma, W. Satterthwaite, M. O'Farrell, S. Hayes, J. Harding, W.J. Sydeman, S.A. Thompson, P. Warzybok, R. Bradley, J. Jahncke, R.T. Golightly, S.R. Schneider, R.M. Suryan, A.J. Gladics, C.A. Horton, S.Y. Kim, S.R. Melin, R.L. DeLong, and J. Abell (2012), State of the California Current 2011-2012: Ecosystems Respond to Local Forcing as La Nina Wavers and Wanes, *California Cooperative Oceanic Fisheries Investigations Reports*, *53*, 41-76.

Bograd, S.J., M.P. Buil, E. Di Lorenzo, C.G. Castro, I.D. Schroeder, R. Goericke, C.R. Anderson, C. Benitez-Nelson, and F.A. Whitney (2015), Changes in source waters to the Southern California Bight, *Deep-Sea Research Part Ii-Topical Studies in Oceanography*, *112*, 42-52.

Bond, N.A., M.F. Cronin, H. Freeland, and N.J. Mantua (2015), Causes and impacts of the 2014 warm anomaly in the NE Pacific, *Geophysical Research Letters*, *42* (9), 3414-3420.

Bray, N.A., A. Keyes, and W.M.L. Morawitz (1999), The California Current system in the Southern California Bight and the Santa Barbara Channel, *Journal of Geophysical Research-Oceans*, *104* (C4), 7695-7714.

Campbell, J.W. (1995), The lognormal-distribution as a model for biooptical variability in the sea, *Journal of Geophysical Research-Oceans*, *100* (C7), 13237-13254.

Carr, M.E., and E.J. Kearns (2003), Production regimes in four Eastern Boundary Current systems, *Deep-Sea Research Part Ii-Topical Studies in Oceanography*, *50* (22-26), 3199-3221.

Chao, Y., M. Ghil, and J.C. McWilliams (2000), Pacific interdecadal variability in this century sea surface temperatures, *Geophysical Research Letters*, *27* (15), 2261-2264.

Cloern, J.E. (2001), Our evolving conceptual model of the coastal eutrophication problem, *Marine Ecology - Progress Series*, *210*, 223-253.

Cullen, J.J. (2015), Subsurface Chlorophyll Maximum Layers: Enduring Enigma or Mystery Solved?, *Annual Review of Marine Science, Vol 7*, *7*, 207-239.

Di Lorenzo, E. (2015), CLIMATE SCIENCE The future of coastal ocean upwelling, *Nature*, *518* (7539), 310-311.

Di Lorenzo, E., V. Combes, J.E. Keister, P.T. Strub, A.C. Thomas, P.J.S. Franks, M.D. Ohman, J.C. Furtado, A. Bracco, S.J. Bograd, W.T. Peterson, F.B. Schwing, S. Chiba, B. Taguchi, S. Hormazabal, and C. Parada (2013), Synthesis of Pacific Ocean Climate and Ecosystem Dynamics, *Oceanography*, *26* (4), 68-81.

Di Lorenzo, E., J. Fiechter, N. Schneider, A. Bracco, A.J. Miller, P.J.S. Franks, S.J. Bograd, A.M. Moore, A.C. Thomas, W. Crawford, A. Pena, and A.J. Hermann (2009), Nutrient and salinity decadal variations in the central and eastern North Pacific, *Geophysical Research Letters*, *36*.

Di Lorenzo, E., and N.J. Mantua (2016), Multi-year persistence of the 2014/15 North Pacific marine heatwave, *Nature Climate Change*, *6* (11), 1042-+.

Di Lorenzo, E., N. Schneider, K.M. Cobb, P.J.S. Franks, K. Chhak, A.J. Miller, J.C. McWilliams, S.J. Bograd, H. Arango, E. Curchitser, T.M. Powell, and P. Riviere (2008), North Pacific Gyre Oscillation links ocean climate and ecosystem change, *Geophysical Research Letters*, *35* (8).

Dorman, C.E., and C.D. Winant (1995), Buoy observations of the atmosphere along the west coast of the United States, *Journal of Geophysical Research-Oceans*, *100* (C8), 16029-16044.

Emery, W.J., and R.E. Thomson (2014), *Data Analysis Methods in Physical Oceanography*, 716 pp., Elsevier Science, Amsterdam.

Flament, P. (2002), A state variable for characterizing water masses and their diffusive stability: spiciness, *Progress in Oceanography*, *54* (1-4), 493-501.

Freeland, H., K. Denman, C.S. Wong, F. Whitney, and R. Jacques (1997), Evidence of change in the winter mixed layer in the Northeast Pacific Ocean, *Deep-Sea Research Part I-Oceanographic Research Papers*, *44* (12), 2117-2129.

Hastie, T., and R. Tibshirani (1986), Generalized Additive Models, *Statistical Science*, *1* (3), 297-310.

Hayward, T.L., T.R. Baumgartner, D.M. Checkley, R. Durazo, G. Gaxiola-Castro, K.D. Hyrenbach, A.W. Mantyla, M.M. Mullin, T. Murphree, F.B. Schwing, P.E. Smith, and M.J. Tegner (1999), The state of the California Current in 1998-1999: Transition to cool-water conditions, *California Cooperative Oceanic Fisheries Investigations Reports*, *40*, 29-62.

Hickey, B.M. (1979), The California Current system: Hypotheses and facts, *Progress in Oceanography*, *8*, 191-279.

Hickey, B.M. (1993), Physical oceanography, in *Ecology of the Southern California Bight*, edited by M.D. Dailey, D.J. Reish, and J.W. Anderson, pp. 19-70, University of California Press, Berkeley.

Howard, M.D.A., M. Sutula, D.A. Caron, Y. Chao, J.D. Farrara, H. Frenzel, B. Jones, G. Robertson, K. McLaughlin, and A. Sengupta (2014), Anthropogenic nutrient sources rival natural sources on small scales in the coastal waters of the Southern California Bight, *Limnology and Oceanography*, *59* (1), 285-297.

Kahru, M., R.M. Kudela, M. Manzano-Sarabia, and B.G. Mitchell (2012), Trends in the surface chlorophyll of the California Current: Merging data from multiple ocean color satellites, *Deep-Sea Research Part Ii-Topical Studies in Oceanography*, *77-80*, 89-98.

Kilduff, D.P., E. Di Lorenzo, L.W. Botsford, and S.L.H. Teo (2015), Changing central Pacific El Ninos reduce stability of North American salmon survival rates, *Proceedings of the National Academy of Sciences of the United States of America*, *112* (35), 10962-10966.

Kim, H.-J., and A.J. Miller (2007), Did the thermocline deepen in the California current after the 1976/77 climate regime shift?, *Journal of Physical Oceanography*, *37* (6), 1733-1739.

Longhurst, A.R. (1995), Seasonal cycles of pelagic production and consumption, *Progress in Oceanography*, *36* (2), 77-167.

Longhurst, A.R. (1998), *Ecological Geography of the Sea*, 398 pp., Academic Press, San Diego.

Lynn, R.J., and J.J. Simpson (1987), The California Current System: The seasonal variability of its physical characteristics, *Journal of Geophysical Research-Oceans*, *92* (C12), 12947-12966.

Mantua, N.J., S.R. Hare, Y. Zhang, J.M. Wallace, and R.C. Francis (1997), A Pacific Interdecadal Climate Oscillation with impacts on salmon production, *Bulletin of the American Meteorological Society*, *78* (6), 1069-1079.

McClatchie, S., R. Goericke, A. Leising, T.D. Auth, E. Bjorkstedt, R.R. Robertson, R.D. Brodeur, X.N. Du, E.A. Daly, C.A. Morgan, F.P. Chavez, A.J. Debich, J. Hildebrand, J. Field, K. Sakuma, M.G. Jacox, M. Kahru, R. Kudela, C. Anderson, B.E. Lavaniegos, J. Gomez-Valdes, S.P.A. Jimenez-Rosenberg, R. McCabe, S.R. Melin, M.D. Ohman, L.M. Sala, B. Peterson, J. Fisher, I.D. Schroeder, S.J. Bograd, E.L. Hazen, S.R. Schneider, R.T. Golightly, R.M. Suryan, A.J. Gladics, S. Loredo, J.M. Porquez, A.R. Thompson, E.D. Weber, W. Watson, V. Trainer, P. Warzybok, R. Bradley, and J. Jahncke (2016), State of the California Current 2015-16: Comparisons with the 1997-98 El Nino, *California Cooperative Oceanic Fisheries Investigations Reports*, *57*.

Meinvielle, M., and G.C. Johnson (2013), Decadal water-property trends in the California Undercurrent, with implications for ocean acidification, *Journal of Geophysical Research-Oceans*, *118* (12), 6687-6703.

Messie, M., and F.P. Chavez (2015), Seasonal regulation of primary production in eastern boundary upwelling systems, *Progress in Oceanography*, *134*, 1-18.

Miller, A.J., and N. Schneider (2000), Interdecadal climate regime dynamics in the North Pacific Ocean: theories, observations and ecosystem impacts, *Progress in Oceanography*, *47* (2-4), 355-379.

Newman, M., M.A. Alexander, T.R. Ault, K.M. Cobb, C. Deser, E. Di Lorenzo, N.J. Mantua, A.J. Miller, S. Minobe, H. Nakamura, N. Schneider, D.J. Vimont, A.S. Phillips, J.D. Scott, and C.A. Smith (2016), The Pacific Decadal Oscillation, Revisited, *Journal of Climate*, *29* (12), 4399-4427.

Nezlin, N.P., M.A. Sutula, R.P. Stumpf, and A. Sengupta (2012), Phytoplankton blooms detected by SeaWiFS along the central and southern California coast, *Journal of Geophysical Research-Oceans*, *117* (C07004), 1-14.

Papadakis, J.E. (1981), Determination of the wind mixed layer by an extension of Newton's method, Vol. 81-9 edited by, in *Pacific Marine Sci. Rep.*, Institute of Ocean Sciences, Sidney, BC, Canada, pp. 32.

Parsons, T.R., Y. Maita, and C.M. Lalli (1984), *A Manual of Chemical and Biological Methods for Seawater Analysis*, 173 pp., Pergamon Press, Oxford.

Patti, B., C. Guisande, A.R. Vergara, I. Riveiro, I. Maneiro, A. Barreiro, A. Bonanno, G. Buscaino, A. Cuttitta, G. Basilone, and S. Mazzola (2008), Factors responsible for the differences in satellite-based chlorophyll a concentration between the major global upwelling areas, *Estuarine Coastal and Shelf Science*, *76* (4), 775-786.

Pebesma, E.J. (2012), Spacetime: spatio-temporal data in R, *Journal of Statistical Software*, *51* (7).

Peterson, W.T., and F.B. Schwing (2003), A new climate regime in northeast pacific ecosystem, *Geophysical Research Letters*, *30* (17).

Philander, G. (1990), *El Nino, La Nina and the Southern Oscillation*, 293 pp., Academic Press, San Diego.

Polovina, J.J., J.P. Dunne, P.A. Woodworth, and E.A. Howell (2011), Projected expansion of the subtropical biome and contraction of the temperate and equatorial upwelling biomes in the North Pacific under global warming, *Ices Journal of Marine Science*, *68* (6), 986-995.

Polovina, J.J., E.A. Howell, and M. Abecassis (2008), Ocean's least productive waters are expanding, *Geophysical Research Letters*, *35* (3), L03618.

Preisendorfer, R.W. (1988), *Principal component analysis in meteorology and oceanography*, 425 pp., Elsevier Science, New York, NY.

Roemmich, D., and J.A. McGowan (1995), Climatic warming and the decline of zooplankton in the California Current, *Science*, *267* (5202), 1324-1326.

Rykaczewski, R.R., and J.P. Dunne (2010), Enhanced nutrient supply to the California Current Ecosystem with global warming and increased stratification in an earth system model, *Geophysical Research Letters*, *37*.

Sarmiento, J.L., R. Slater, R. Barber, L. Bopp, S.C. Doney, A.C. Hirst, J. Kleypas, R. Matear, U. Mikolajewicz, P. Monfray, V. Soldatov, S.A. Spall, and R. Stouffer (2004), Response of ocean ecosystems to climate warming, *Global Biogeochemical Cycles*, *18* (3).

Simpson, G. (2014), Identifying periods of change in time series with GAMs.

Steinacher, M., F. Joos, T.L. Frolicher, L. Bopp, P. Cadule, V. Cocco, S.C. Doney, M. Gehlen, K. Lindsay, J.K. Moore, B. Schneider, and J. Segschneider (2010), Projected 21st century decrease in marine productivity: a multi-model analysis, *Biogeosciences*, *7* (3), 979-1005.

Sydeman, W.J., J.A. Santora, S.A. Thompson, B. Marinovic, and E. Di Lorenzo (2013), Increasing variance in North Pacific climate relates to unprecedented ecosystem variability off California, *Global Change Biology*, *19* (6), 1662-1675.

Thomson, R.E., and I.V. Fine (2003), Estimating mixed layer depth from oceanic profile data, *Journal of Atmospheric and Oceanic Technology*, *20* (2), 319-329.

Trenberth, K.E. (1997), The definition of El Nino, *Bulletin of the American Meteorological Society*, *78* (12), 2771-2777.

Wang, S., J. Huang, Y. He, and Y. Guan (2014), Combined effects of the Pacific Decadal Oscillation and El Niño-Southern Oscillation on Global Land Dry–Wet Changes, *Scientific Reports*, *4*, 6651.

Wood, S.N. (2016), Just Another Gibbs Additive Modeler: Interfacing JAGS and mgcv, *Journal of Statistical Software*, *75* (7), 1-15.

Zhang, Y., J.M. Wallace, and D.S. Battisti (1997), ENSO-like interdecadal variability: 1900-93, *Journal of Climate*, *10* (5), 1004-1020.